

Article

Low-Calcium, Porous, Alkali-Activated Materials as Novel pH Stabilizers for Water Media

Laura Vitola ^{1,*} , Diana Bajare ¹, Angel Palomo ² and Ana Fernandez-Jimenez ² 

¹ Department of Building Materials and Products, Institute of Materials and Structure, Riga Technical University, Kalku Street 1, LV-1658 Riga, Latvia; diana.bajare@rtu.lv

² Department of Materials, Eduardo Torroja Institute for Construction Science, 28033 Madrid, Spain; palomo@ietcc.csic.es (A.P.); anafj@ietcc.csic.es (A.F.-J.)

* Correspondence: laura.vitola_1@rtu.lv

Received: 31 August 2020; Accepted: 19 October 2020; Published: 22 October 2020



Abstract: Due to the increase of water consumption, water treatment systems become more actual and innovative materials for water treatment are welcomed. Traditionally, alkalizing agents, such as lime or caustic soda, have been employed to increase the pH levels, which induce chemical clarification of wastewater. Some innovative ideas of using low-calcium, alkali-activated materials (AAM) for this purpose have been considered previously. In this study, the low-calcium, porous, alkali-activated material (pAAM) was characterized to understand the impact of the aluminum silicate source and heat treatment on basic properties for material that might be used in water treatment systems as a softener by stabilizing the pH. The studied porous alkali-activated materials may ensure stable and long-lasting (30 days) pH (pH 10.3–11.6) in water media depending on the composition and amount of activation solution used for AAM preparation. Heat treatment does not have an impact on the mineralogical composition and structural properties of the pAAM, but it does change the leaching ability of alkalis from the material structure.

Keywords: porous alkali-activated materials; pH stabilizing; zeolites

1. Introduction

According to global water security data, world water consumption has increased from 600 billion m³ to 4600 billion m³ in the last 17 years [1]. This indicates that water treatment is becoming increasingly important. In order to optimize the water treatment systems, it is more efficient to use materials ensuring stable alkaline media (pH 9.5–11.5) for longer time period. Particles, colloids, and certain dissolved materials present in the wastewater can be efficiently removed by using flocculation processes at high pH. Traditionally, alkalizing agents, such as lime or caustic soda, have been employed to increase the pH levels, which induce chemical clarification of wastewaters [1]. However, more recently, some papers have been published in which the idea of using low-calcium, alkali-activated materials (AAM) for this purpose has also been considered with some promising results [2–6].

The way alkalis take part in the activation process in alkali-activated materials (AAM) can be divided into three groups. First of all, part of alkalis is incorporated into the main reaction product (the sodium aluminosilicate hydrate (N-A-S-H) gel) to balance the negative charge [7]. Another part appears incorporated into zeolites (formed as second reaction product) [8]. The rest of alkalis are free in the pore solution. It has been demonstrated that the pore solution in AAM contains a high concentration of OH⁻, typically more than 500 mM and in several cases even greater than 1 M [9]. Those free alkalis are available for leaching [9], allowing the use of AAM as pH buffering materials. Also, high concentration of free alkalis in contact with water or solutions may cause the efflorescence [10]. In many cases,

the leaching rate of Na^+ and OH^- from the structure of AAM activated with NaOH or modified sodium silicate solution is high for the first few weeks, decreasing in time [3,5]. The leaching of alkalis is affected by three main factors: Chemical composition of raw materials (type of precursor and activator, alkali activator solution/solid ratio), physical properties (porosity, pore structure), and production method of AAM (curing conditions, thermal treatment, etc.) [2,5,11–13]. The previous results from different studies have shown that calcined illite clay [3], biomass-fly ash [5], natural zeolite [14], glass waste and slag blend [15], and metakaolin [2,16] can be used as raw materials for production of AAM.

It is well known that zeolites and zeolite-like materials are used as pH stabilizers and unwelcomed chemical compound absorbents in water treatment systems [17–19]. It is proven that AAM can contain a certain amount of zeolite, depending on the chemical composition of the precursors and activation solution used as well as from the curing conditions. Zeolite Na-A, hydrosodalite, zeolite X, faujasite, analcime, and other types of zeolites of different sizes and amounts can be found in the structure of AAM as a secondary alkali activation reaction product [7,20–23]. Zeolites in the structure of AAM could improve the effectiveness of contamination sorption from wastewater, such as heavy metals [24–26], ammonium [27], calcium [25], and fluoride [18]. Due to relatively weakly bonded alkali atoms in the N-A-S-H gel structure (similar to zeolites) it is possible to provide a Na^+ and OH^- ion exchange in water media [28].

Alkali-activated materials with high porosity could be used for water treatment systems as pH adjustment materials due to its stable alkali leaching rate in time as well as its intensity of ion exchange due to a high specific surface. There are different foaming agents that can be used to produce porous alkali-activated materials (pAAM): Hydroxide peroxide [5,29]; an aluminum paste [3,28,30] foaming agent, for example, sodium dodecyl sulphate [31,32]; aluminum containing, for example, aluminum scrap recycling waste [33]; Na-perborate monohydrate [34]; and others. The high pH buffering capacity of pAAM in water media has been reported by Novais et al. [5,6] as well as by Bajare and Bumanis [11]. The maximum leached alkalis from the biomass-fly ash-based pAAM granules during a 25-day period were 0.032 mol/(L·g) [5], which is substantially higher comparing to biomass-fly ash pAAM monoliths (0.018 mol/(L·g)) reported by Novais et al. [6]. Meanwhile, for the granules of glass-modified pAAM based on metakaolin reported by Bajare and Bumanis it was 0.027 mol/(L·g) during a 25-day period [11].

Nevertheless, additional research would shed light on the parameters mainly affecting the alkali's leaching and ion exchange of pAAM in the water media. In particular, the influence of the chemical composition of raw materials on the leaching ability of pAAM remains unclear. For this paper, different raw materials were used: Fly ash (FA), metakaolin (MK), and a mixture of both (4/6). Porous monolithic materials and granules were produced for the planned tests. To determine the effect of thermal treatment considered as an effective treatment for the changing of alkali leaching ability and its ability to ensure stable pH over time in water media [3,28], some samples were treated at 200 °C for 3 h.

2. Materials and Methods

2.1. Raw Materials

Fly ash (FA) (class F in accordance to the ASTM standard C618–03 [35]) and metakaolin (MK) were used as aluminum silicate sources. FA was taken from the Teruel thermoelectric plant in Spain, which uses coal as a combustible. It was ground for 30 min in a ball grinding machine before use and 75% of its particles were smaller than 45 μm . FA had a mainly vitreous phase, but some minor crystalline phases such as mullite ($\text{Al}_6\text{Si}_2\text{O}_{13}$), hematite (Fe_2O_3), and quartz (SiO_2) were detected by XRD (XRD diffractogram is shown in the Results section).

The MK was obtained through the calcination of kaolin from Guadalajara for 2 h at 750 °C. The original kaolin was already ground with 80% of the particles with a size less than 45 μm . The chemical composition of the solid raw materials was detected by quantitative X-ray fluorescence (XRF) using a PHILIPS PW-1004-ray spectrometer (Eindhoven, the Netherlands) (Table 1). To determine

the amount of reactive silica and alumina in the raw materials, a selective chemical attack with 1% (V/V) hydrofluoric acid solution was done according to Ruiz-Santaquiteria et al. [36]. The obtained data is included in Table 2. MK presented an amorphous phase with some minor crystalline phase quartz (SiO₂) (XRD diffractogram is shown in Results).

Table 1. Chemical composition of solid raw materials (wt.%).

Chemical Compounds	FA	MK	* FA + MK
SiO ₂	39.03 ** 36.61	53.74 ** 38.55	45.06 ** 37.41
Al ₂ O ₃	27.06 ** 15.47	44.47 ** 33.49	34.20 ** 22.86
Fe ₂ O ₃	19.5	0.45	11.69
CaO	6.4	0.21	3.86
K ₂ O	1.04	0.55	0.84
TiO ₂	0.96	0.10	0.61
MgO	1.04	0.10	0.65
Na ₂ O	0.16	0.00	0.09
Others	2.56	0.18	1.59
LOI, 1000 °C	2.25	0.2	1.41
Sum	100.00	100.00	100.00

* The FA + MK proportion of FA and MK was 41% and 59%, respectively. ** Reactive oxides determined by acid attack [36].

Table 2. Compositions of studied samples and amount of main oxides in pastes.

Name of Sample	Mixture Design, Mass Part					Main Oxides in Pastes, % in Weight						
	MK	FA	Activator	Foaming Agent P	L/S	From Precursor		From Activator		Ratios		
						SiO ₂	Al ₂ O ₃	Na ₂ O	SiO ₂	SiO ₂ /Al ₂ O ₃	SiO ₂ /Na ₂ O	Al ₂ O ₃ /Na ₂ O
FA_0	0.00	1.00	0.32	0.015	0.32	^a 27.77 ^c 19.92	^a 22.98 ^c 17.31	^b 8.73	^b 1.28	^a 1.26 ^c 1.23	^a 3.33 ^c 2.43	^a 2.63 ^c 1.98
MK_0	1.00	0.00	0.92	0.015	0.92	^a 27.77 ^c 19.92	^a 22.98 ^c 17.31	^b 8.73	^b 1.28	^a 1.26 ^c 1.23	^a 3.33 ^c 2.43	^a 2.63 ^c 1.98
FA + MK_0	0.41	0.59	0.57	0.015	0.57	^a 28.43 ^c 23.60	^a 21.58 ^c 14.42	^b 6.60	^b 0.97	^a 1.36 ^c 1.70	^a 4.45 ^c 3.72	^a 3.27 ^c 2.18

^a from bulk composition; ^b from activator; ^c reactive oxide concentration determined by acid attack [36].

A modified 8 M NaOH solution with a sodium metasilicate solution (mass ratio 9/1) was used as an activator. The total amount of Na₂O and SiO₂ in the activator was 18.4% and 2.7%, respectively. The pH of the activator used was 13.35 and its density at room temperature was 1.28 g/cm³ and at 5 °C it was 1.31 g/cm³.

The structure of pAAM was obtained using a commercially available pore formation agent, hydrogen peroxide (produced by Panreac, 30% W/V (100 VOL.)).

2.2. Mixture Design and Sample Preparation

The mixture design of pAAM is shown in Table 2. All raw materials were kept at +5 °C for 24 h before the samples were prepared to slow down the reaction between the blowing agent P (H₂O₂) and the activator to gain extra time for paste mixing. The liquid/solid ratio (L/S) was chosen according to the results of the pre-research with an aim to finding an optimal consistency of fresh paste to ensure the setting of the pAAM and to obtain maximally high porosity after the blowing agent P (H₂O₂) was added. A different amount of activator had to be added to the solid precursor to ensure the correct workability of the paste. The liquid/solid ratio (L/S) of the paste was based on MK (L/S = 0.92), which was higher than that of the paste based on FA (L/S = 0.32), while the L/S of the paste made from the FA and MK blend was 0.57 (Table 2) and depended on the particle sizes of the raw materials.

The blend of raw materials and the activator was mixed for 1.5 min slowly and 1.5 min quickly using a mechanical mixer. The P (H_2O_2) was added to the composition after homogenous paste was obtained. The slow mixing was continued for an additional 10 s. Immediately afterwards, the paste-preparing molds ($40\text{ mm} \times 160\text{ mm} \times 160\text{ mm}$) were filled and kept at room temperature ($20\text{--}23\text{ }^\circ\text{C}$). The structure of pAAM was formatted before the paste started to set. After 30 min, the specimens were put in the oven and cured at $85\text{ }^\circ\text{C}$ for 20 h.

After, two series of samples were prepared: Type I—FA_0, MK_0, MK + FA_0 without heat treatment and type II—FA_200, MK_200, MK + FA_200 with heat treatment at $200\text{ }^\circ\text{C}$ for 3 h (Figure 1). Monolithic cubes ($40\text{ mm} \times 40\text{ mm} \times 40\text{ mm}$) and granules (2–4 mm) were prepared from the obtained samples ($40\text{ mm} \times 160\text{ mm} \times 160\text{ mm}$) before and after the heat treatment (Figure 2). Cubes were obtained using a hacksaw machine and granules were obtained by mechanical crushing and sieving through 2 mm and 4 mm sieves. After the mechanical test, the samples were ground into powder for the next tests, with a determination of the true density, XRD, FTIR, and TG/DTG.

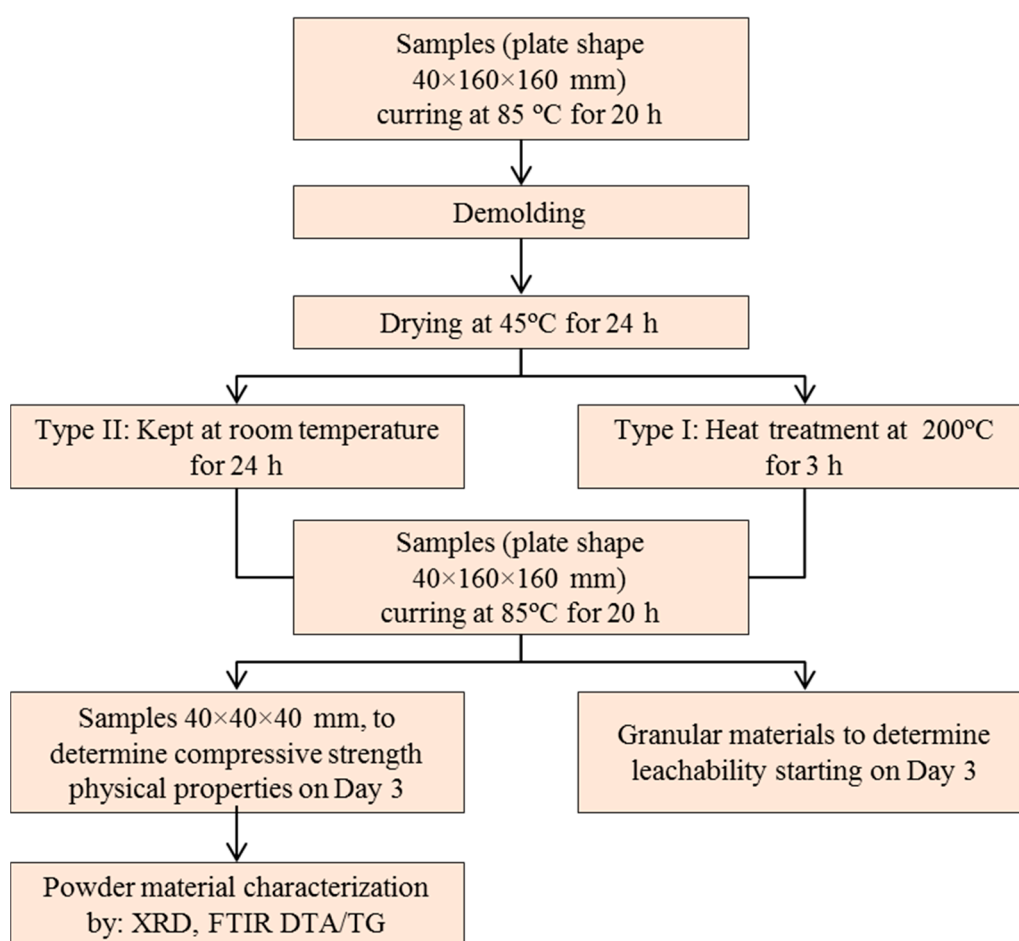


Figure 1. Scheme of sample testing.

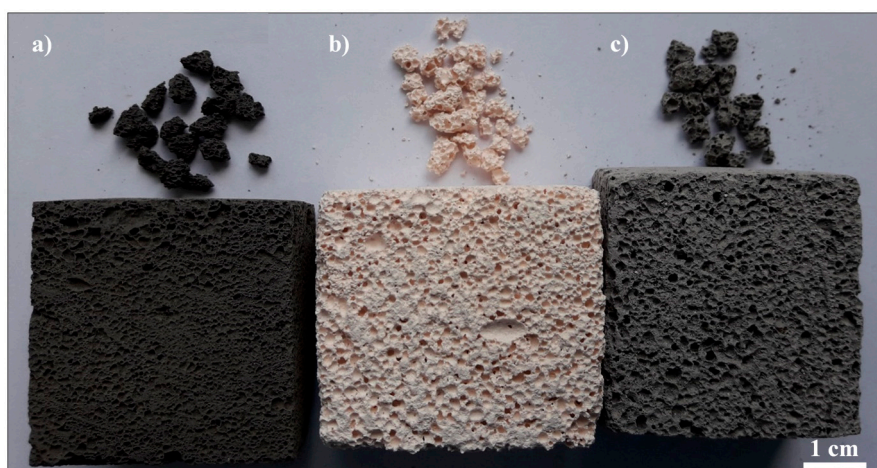


Figure 2. Porous structure of obtained monolithic pAAM and prepared pAAM granules for leaching test: (a) FA_0, (b) MK_0, (c) FA + MK_0.

2.3. Techniques

The cubical samples (40 mm × 40 mm × 40 mm) of pAAM were used for the testing of physical properties (bulk density and water absorption (wt.%)). The bulk density was calculated as the mass and volume division of samples. Water absorption by mass was determined using the following method: Dry samples were measured and totally immersed in water for seven days; the mass changes after seven days were defined as water absorption by mass [37]. The open porosity by volume was calculated as the absorbed water volume and dry sample volume division in percentages. The le Chatelier flask was used to determine the true density of the powder pAAM and the total porosity (vol.%) of pAAM was calculated in accordance with ASTM C188 [38]. The compressive strength was tested using 3-day-old samples (before and after the heat treatment at 200 °C) and 10-day-old samples (before and after heat treatment), which were kept in water media for one week. The obtained results were compared to determine the softening of the material.

Thermogravimetric-differential thermal analysis (TG/DTG) was carried out using a Stanton Redcroft STA 781 thermal analyzer (Twin Lakes, WI, USA) at 0–700 °C with a heating rate of 5 °C/min. For XRD characterization, the BRUKER-AXS D8 ADVANCE X-ray diffractometer (Billerica, MA, USA) was used, collected with CuK α 1, α 2 radiation in the range 5–60° (2 θ). The ATIMATTSON FTIR-TM was used to obtain the FTIR spectra with a range of 2000–400 cm⁻¹. Specimens for FTIR were prepared by mixing 300 mg of KBr with 1 mg of the sample. The JEOL JSM 5400 scanning electron microscope (Tokyo, Japan, SEM) with a LINK-ISIS energy dispersive analyzer (Oxford, UK, EDX) was used to characterize the microstructure of pAAM. Parallelepiped-shaped samples (~10 mm × 10 mm × 5 mm) were used for SEM/EDX analysis. EDX data were taken from different points on the surface of sample. The scheme of testing procedures is given in Figure 1.

Granular samples of obtained pAAM (each 3.0 ± 0.2 g) was immersed in the 100 mL of deionized water for 24 h to determine the pH and leaching. Samples were moved to the new batch with deionized water (100 mL) every 24 h. The portable pH/mV meter HI 991003 with sensor check was used to determine the pH of leachates. Obtained leachates were titrated to determine OH⁻ group in (OH⁻ mol/(L·g)) with hydrochloric acid 0.01 M to pH 7.0 for determination of alkalinity.

3. Results and Discussions

3.1. Physical and Mechanical Properties

The physical properties of the monolithic pAAM are shown in Table 3. The bulk density of pAAM was between 460–750 kg/m³, the water absorption by mass was up to 60%, and the total porosity was within the range of 71–79%, depending on material composition. As seen in Table 3, the bulk density

of the obtained pAAM decreased after heat treatment. No volume variation was observed for samples after heat treatment. Therefore, the phenomena that bulk density decreases during heat treatment is associated with the reduction of the sample's mass due to the evaporation of the free water present in the aqueous phase in the structure of the material or in the decomposition of hydration products, as will be seen later in the study by TG/DTG.

Table 3. Physical properties of pAAM.

Name of Samples	Bulk Density, kg/m ³	True Density, kg/m ³	Water Absorption by Mass, %	Total Porosity, %	Open Porosity, %	Closed Porosity, %
FA_0	750 ± 5	2450	40 ± 3	71 ± 1	29 ± 1	42 ± 1
FA_200	680 ± 10	2450	44 ± 5	74 ± 1	31 ± 1	43 ± 1
MK_0	490 ± 15	2160	58 ± 1	77 ± 2	29 ± 2	48 ± 2
MK_200	460 ± 8	2160	60 ± 1	79 ± 1	32 ± 1	47 ± 1
MK + FA_0	550 ± 17	2270	53 ± 4	76 ± 1	25 ± 1	51 ± 1
MK + FA_200	520 ± 15	2270	59 ± 3	77 ± 1	28 ± 1	49 ± 1

Samples based on MK had water absorption using mass on the order of $58 \pm 1\%$, while samples based on FA had up to $40 \pm 3\%$. However, samples made from a mixture of FA and MK were close to $53 \pm 4\%$. Heat treatment increased the water absorption of pAAM. Water absorption of alkali-activated fly ash pAAM increased by 10% after heat treatment at 200 °C, for pAAM made of metakaolin it increased by 3%, and for pAAM made from the activated FA and MK mix, by 11%. The water absorption results represent different quantities for samples with and without heat treatment at 200 °C, given their different thermal histories and removal (or not) of physically bounded water.

The open porosity of pAAM increased after heat treatment (Table 3.). Samples based on FA had an open porosity of 29% (FA_0) and 31% (FA_200). Meanwhile, for samples based on MK the open porosity was 29% (MK_0) and 32% (MK_200), but for the samples based on FA and MK blend, the open porosity was 25% (MK + FA_0) and 28% (MK + FA_200). The increase of open porosity induced by heat treatment at 200 °C temperature can be attributed to the evaporation of water from the structure of the material. A similar behavior was observed for the closed porosity of the obtained samples, which increased from 42 to 51% depending on their composition and heat treatment. Therefore, the total porosity increased by 2–3% (Table 3.).

The compressive strength of pAAM is shown in Figure 3. The samples made from FA had higher compressive strength at day 3 (1.6 MPa before heat treatment (FA_0) and 1.9 MPa after heat treatment (FA_200)) than samples made of MK or of MK + FA mix. Heat treatment did not influence compressive strength of specimens made of MK (0.4 MPa at day 3). The samples based on the FA and MK blend had compressive strength 0.7 MPa before heat treatment and 1.0 MPa after heat treatment.

The compressive strength of 10-day-old samples that were kept in water for seven days increased from 10–25%. It indicates that water media did not have a negative impact on the compressive strength of the obtained pAAM and the softening of materials did not happen. This aspect is very important for materials that are intended to be used in water media. As these results show an increase in strength, it is possible to conclude that formation of the pAAM structure is still continuing. These phenomena should be investigated more deeply in future studies since it is known that the formation of N-A-S-H gel continues for a prolonged time period if there are available water and free alkalis with the rest of the amorphous components from the raw materials [39].

3.2. Reaction Product Characterization

The XRD diffractograms of the pAAM presented the halo at 20–30° 2-theta (Figure 4). The halo at 15–25° found in raw materials moved to a region of higher degree after alkali activation and it corresponded to the N-A-S-H gel formation [40]. This phenomenon was observed for all compositions.

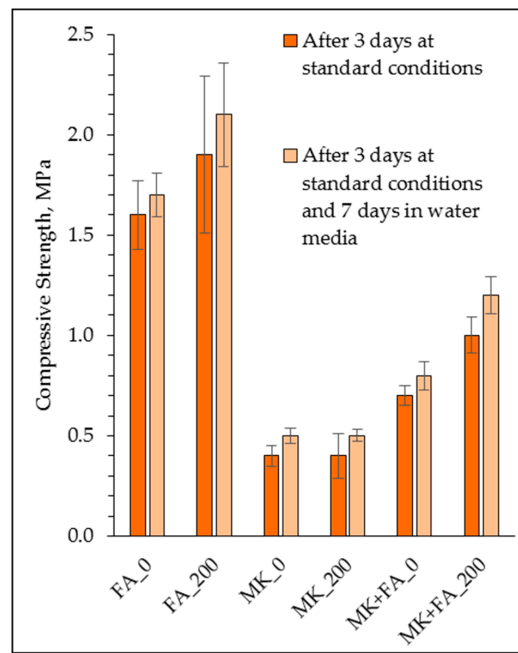


Figure 3. The compressive strength of pAAM on day 3 and day 10 (after seven days in water media).

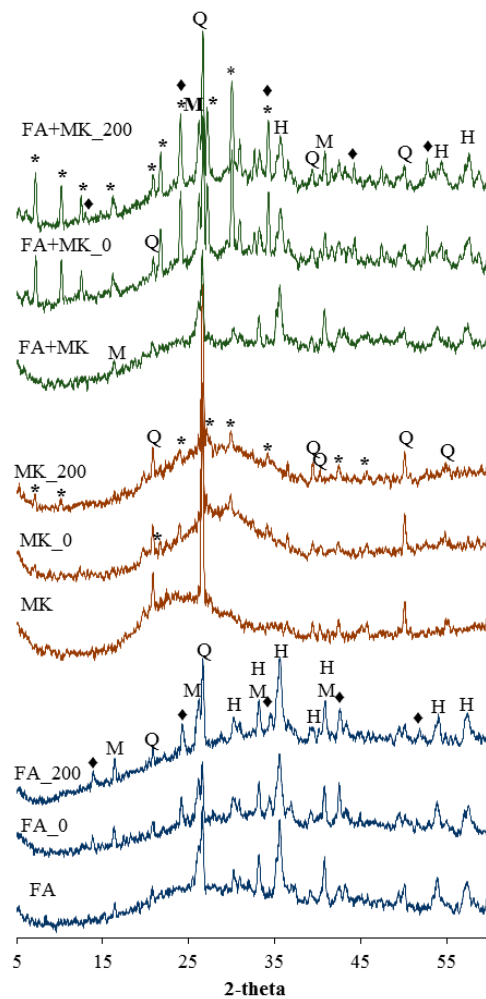


Figure 4. Diffractogram of solid raw materials and obtained pAAM; Q—quartz (87–2096), M—mullite (83–1881), H—hematite (85–0599), *—zeolite 4A (39–0222), ♦—chabazite (19–1178).

The pAAM made from FA has a crystalline phase from the raw FA (quartz, mullite and hematite). The new crystalline phase as chabazite ($\text{NaAlSi}_2\text{O}_6 \cdot 3\text{H}_2\text{O}$, $\text{Si}/\text{Al} = 2$) was detected (Figure 4). The diffractogram of pAAM made from MK (MK_0) showed the presence of quartz (from the original MK) and a small amount of zeolite A ($(\text{Na}_9\text{Al}_9\text{Si}_9\text{O}_{384} \cdot 6\text{H}_2\text{O})$, $\text{Si}/\text{Al} = 1$) (Figure 4). The diffractogram of pAAM made from the FA and MK mixture (MK + FA_0) showed quartz and mullite from the original materials as well as the presence of zeolite A and chabazite (Figure 4). The clear impact of the heat treatment on the obtained pAAM was not detected by XRD, as can be seen in Figure 4. After the heat treatment, the amorphous and crystalline phases of all the samples did not change significantly.

The FTIR spectra of raw materials and obtained pAAM before and after heat treatment are presented in Figure 5. The FTIR spectra of FA consisted of two main intense bands at 1092 cm^{-1} , which corresponded to the asymmetric stretching vibrations of T–O (where T is Si or Al), and at 462 cm^{-1} , which was assigned to the internal T–O bending vibrations [41]. After the activation of the raw materials, the band at 1092 cm^{-1} moved to 993 cm^{-1} because N–A–S–H gel was forming [41,42]. The same was detected for the alkali-activated MK and for the FA and MK blend. The band at 1084 cm^{-1} (in the case of MK) moved to 995 cm^{-1} and the band at 1084 cm^{-1} (in the case of the FA and MK blend) moved to 1002 cm^{-1} after the alkali activation.

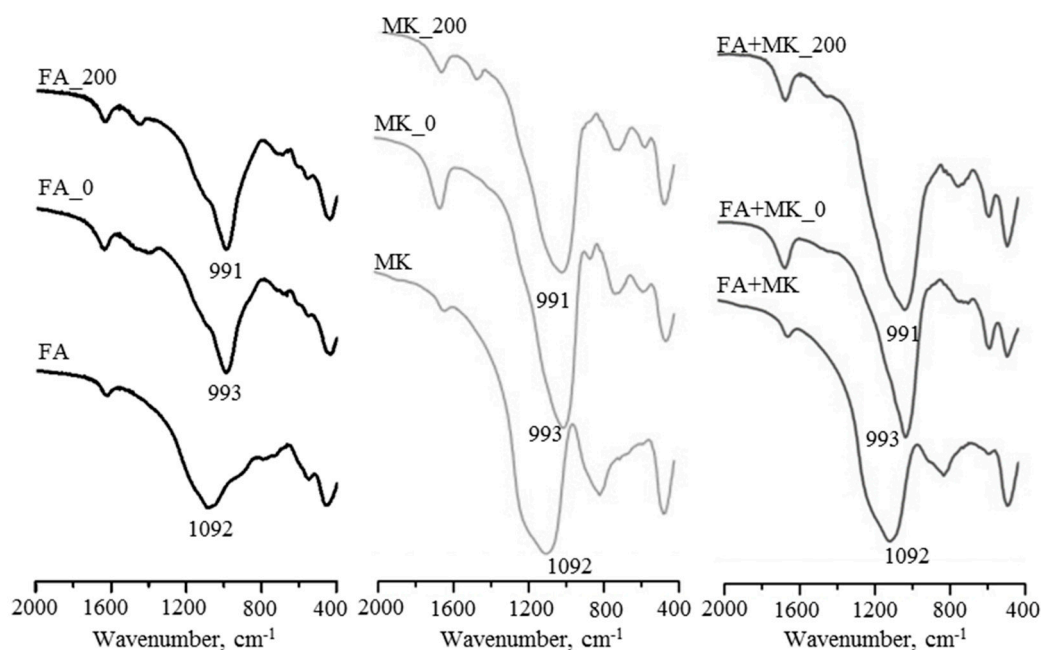


Figure 5. FTIR analyses for solid raw materials and obtained pAAM.

Bands at $553\text{--}571\text{ cm}^{-1}$ are typical of tetrahedral aluminum stretching [43,44]. After the alkali activation of MK and MK + FA, the band at $556\text{--}570\text{ cm}^{-1}$ appeared to be more intensely identified as double four-membered ring vibrations in the zeolite framework [20]. The C–O band asymmetric stretching vibration band, typical of aragonite, appeared at $1420\text{--}1451\text{ cm}^{-1}$ [41] after the heat treatment of the samples, while before the heat treatment, this band appeared only for the sample FA_0 at 1401 cm^{-1} . Bands appearing at $1624\text{--}1650\text{ cm}^{-1}$ were attributed to the O–H bending vibrations in the water molecules [20,44].

After the heat treatment, no significant changes were detected in the FTIR spectra. In the case of the sample based on MK and FA + MK, the main band moved from 995 cm^{-1} to 999 cm^{-1} (in the case of MK) and from 1002 cm^{-1} to 1006 cm^{-1} (in the case of FA + MK). This is explained by the SiO_2 (from raw MK) transformation from the crystalline/semi-crystalline to the amorphous phase as well as the N–A–S–H gel formation during the heat treatment. In the case of the sample based on FA treated at $200\text{ }^\circ\text{C}$, a different phenomenon was detected; the main band at 993 cm^{-1} moved to 991 cm^{-1} .

The macrostructure of AAM before heat treatment in the SEM pictures is shown in Figure 6. Structural changes caused by heat treatment were not detected by SEM. FA_0 had a macroporous structure with a pore size of up to 0.9 mm, while MK_0 and MK + FA_0 had pore sizes up to 2.0 mm. The obtained AAM had a nonhomogeneous porous structure. It was determined that heat treatment at 200 °C had no impact on AAM macrostructure.

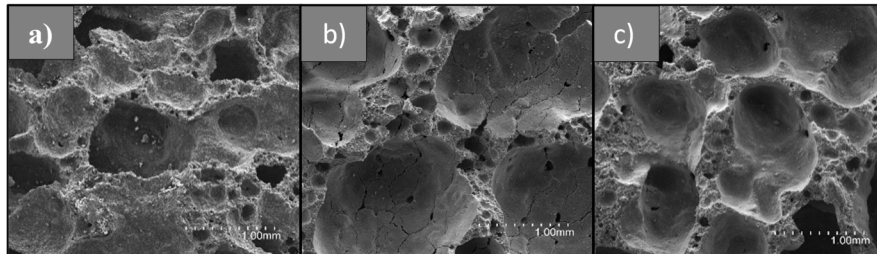


Figure 6. Macrostructure of obtained pAAM, studied by SEM with magnification $\times 30$: (a) FA_0, (b) MK_0, (c) FA + MK_0.

In the microstructure of all samples, it was possible to detect different types of crystals, as seen in Figure 7. Ball-shaped crystals with a diameter of 1.0–2.3 μm , defined as chabazite according to XRD results, were found in the structure of FA_0 (Figure 7a). Irregular dodecahedron-shaped crystals with a diameter from 3.0 to 7.0 μm were detected on the pore surface of MK_0 sample (Figure 7b). It was not possible to detect the mineralogical composition of these crystals by XRD, probably due to its size and low concentration. According to the literature [45], those crystals are defined as analcime crystals. Pore surface of MK + FA_0 was covered with deformed, cube-shaped crystals with a diameter of 1.5–2.0 μm (defined as zeolite A) and ball-shaped crystals with a diameter of 1.0–3.0 μm , similar to those in sample FA_0 (chabazite) (Figure 7c).

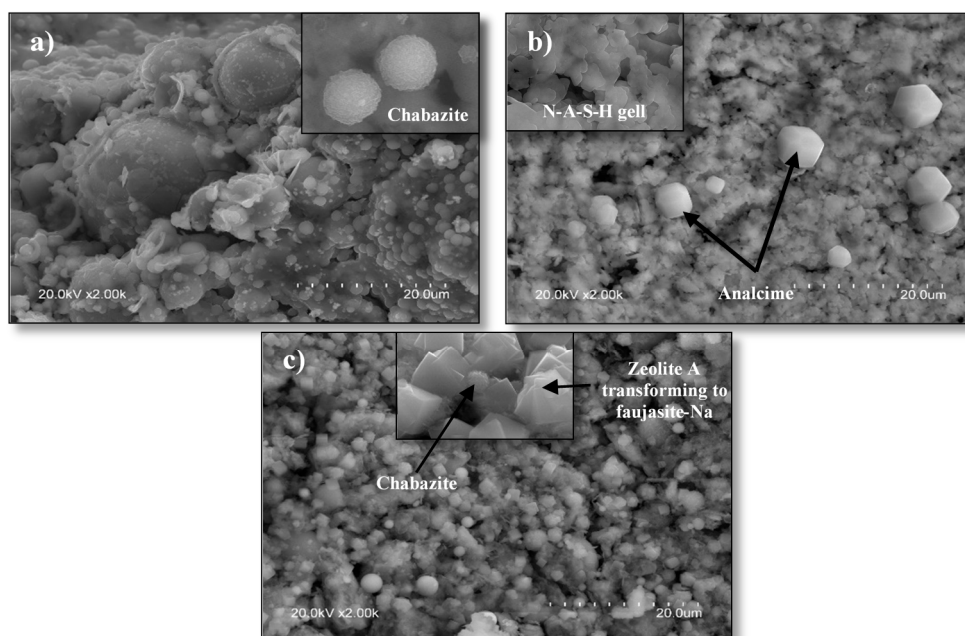


Figure 7. Porous surface-studied pAAM by SEM with magnification $\times 2000$: (a) FA_0, (b) MK_0, (c) FA + MK_0.

As can be seen in Figure 8a, the sample with FA had less sodium and silica in its structure compared to other samples (MK_0 and MK + FA_0). The difference in the amount of sodium can be explained by the L/S ratio used for pAAM preparation (Table 2). The L/S ratio of FA_0 was 0.32, while the L/S ratio

of MK_0 was 0.92 and MK + FA_0 was 0.57. This means that samples made with FA had less sodium in the material composition, which came from the alkali-activation solution or activator. The different amount of silica in each composition depended on the chemical composition of raw materials used for preparation of pAAM (Table 1). FA had less silica oxide than the MK (39.03 versus 53.74%) and more Fe (i.e., 19.05% of Fe_2O_3), while in MK, the Fe_2O_3 was less than 1%.

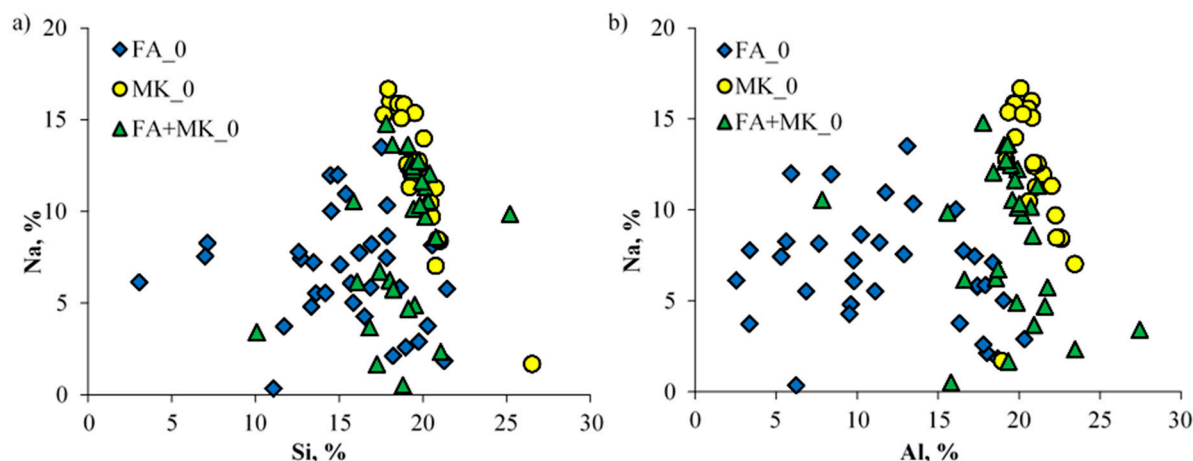


Figure 8. The analysis of pAAM by EDX, correlations between (a) Na and Si amount of each spectra; (b) Na and Al amount of each spectra.

TG/DTG was used to determine changes that appeared during heat treatment of pAAM. The TG/DTG curves of the obtained material are given in Figure 9. It focused on the changes detected between 25 °C and 200 °C. The peak maximum of the DTG curve at 98 °C temperature represented the water loss of FA_0, which constituted 5.2% of the weight loss, while MK_0 at 129 °C and MK + FA_0 at 127 °C constituted 11.5% (MK_0) and 8.9% (MK + FA_0), respectively. The weight loss of pAAM between 25 °C and 150 °C was associated with the evaporation of physically bonded water from the pore structure [28] as well as with different L/S ratios used for sample preparation (Table 2). The paste of MK_0 had 2.0 times more water coming from the activator in its composition than sample FA_0 and 1.5 times more than sample MK + FA_0.

3.3. Leaching Behavior

The leaching test results indicated that all studied pAAM samples ensured $\text{pH} \geq 10$ up to 30 days (Figure 10). The pAAM made from FA provided continuous decrease of pH up to 30 days in water media (from pH 11.6 to 10.3 FA_0), while MK-based pAAM provided pH 11.1 (on day 1) and decreased to 10.5 on day 30. The pAAM based on MK + FA had a similar result as pAAM based on MK. The initial pH was 11.4 (on day 1) and it decreased to 10.5 on day 35 (Figure 10). The effect of the heat treatment of pAAM had a small impact on the pH adjustment in water media during the testing period (30 days).

According to the evidence shown in Table 2, it can be argued that pAAM with FA had two times fewer alkalis to leach out into the water media compared to pAAM with MK and 1.5 times fewer than pAAM with FA + MK. Samples with an FA crystalline structure were observed (Figure 4), i.e., the pAAM with FA had more zeolites and less N-A-S-H gel in their structure compared to pAAM with MK and FA + MK. During the first days of the test, the pH level was maintained using free alkalis from a porous solution. Then zeolites and N-A-S-H gel provided the alkaline pH level. The pAAM with MK and FA + MK had more alkalis in total (Table 2), relatively more N-A-S-H gel during the alkali-activation process (Figure 4), and slightly higher closed porosity (Table 3), thus ensuring that the alkalis were gradually released from the pAAM structure.

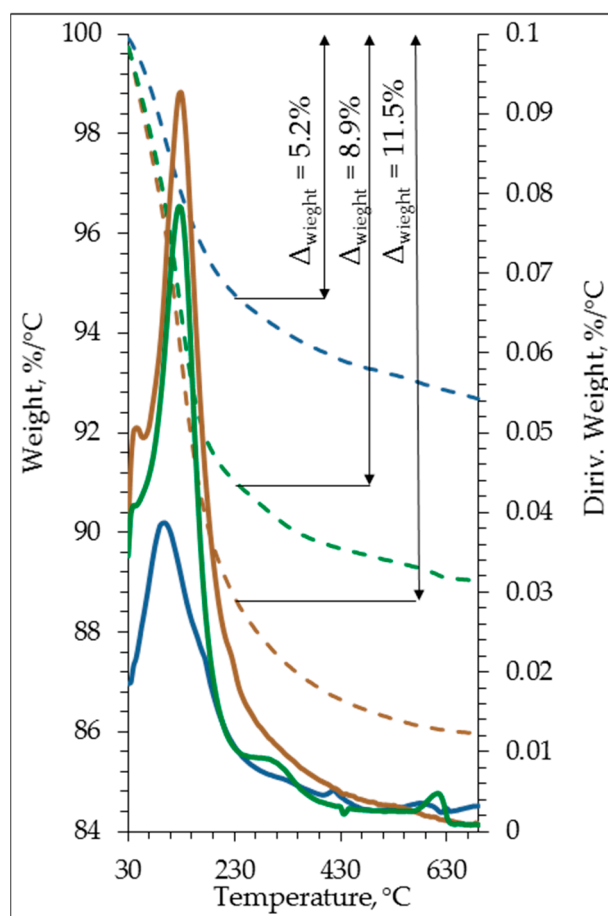


Figure 9. TG/DTG of obtained porous AAM (dashed—TG, solid—DTG): FA_0—blue, MK_0—brown, FA+MK_0—green.

As seen in Figure 11, the heat treatment had effect on the leaching properties of the studied pAAM, depending on the composition (Table 2). The amount of leached OH^- ion from the structure of pAAM depended on the type of aluminum silicate source (FA, MK, or MK + FA) used as a base material to obtain pAAM. The pAAM with FA (FA_0) leached out 0.036 OH^- (mol/(L·g)) after a 30-day leaching test, while pAAM with MK (MK_0) leached out 0.019 OH^- (mol/(L·g)), and pAAM with MK and FA (MK + FA_0) leached out 0.025 OH^- (mol/(L·g)) (Figure 10a). The chemical composition of the aluminum silica sources provided different $\text{SiO}_2/\text{Al}_2\text{O}_3$ ratios (Table 2), which could influence OH^- leaching from the pAAM structure. Mixture compositions for pAAM with FA had an increased reactive $\text{SiO}_2/\text{Al}_2\text{O}_3$ ratio (2.4) compared to pAAM with MK (1.2), which impacted the leaching of OH^- ions. The testing process described above corresponded to the findings of Hong et al. [46].

Noticeable heat treatment impact on leaching properties (Figure 11) was determined in samples that contained MK. Comparing the amount of leached OH^- during the 30 days, it decreased for 26% (from 0.019 to 0.014 mol/(L·g)) for heat treated samples, but still pH adjustment in water media was similar (Figure 10). It means that pH adjustment performance for heat treated samples was higher and, taking into account that amount of alkalis used in the sample preparation was the same, the adjustment will be long-lasting compared with samples that were not treated.

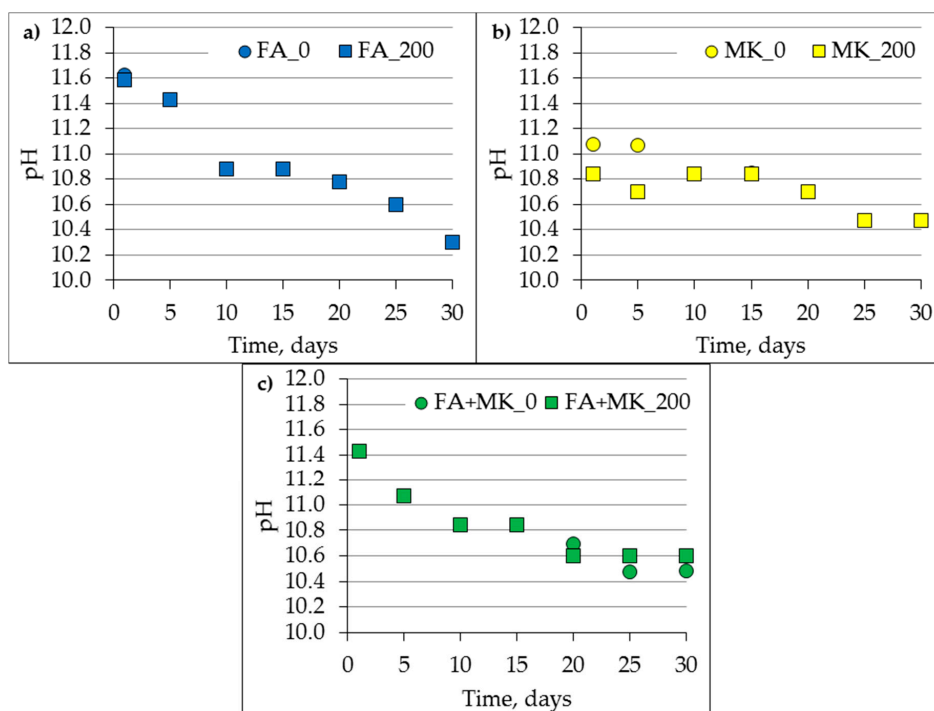


Figure 10. The pH changes in time (a) for samples FA_0 and FA_200; (b) for samples MK_0 and MK_200; (c) for samples FA + MK_0 and FA + MK_200.

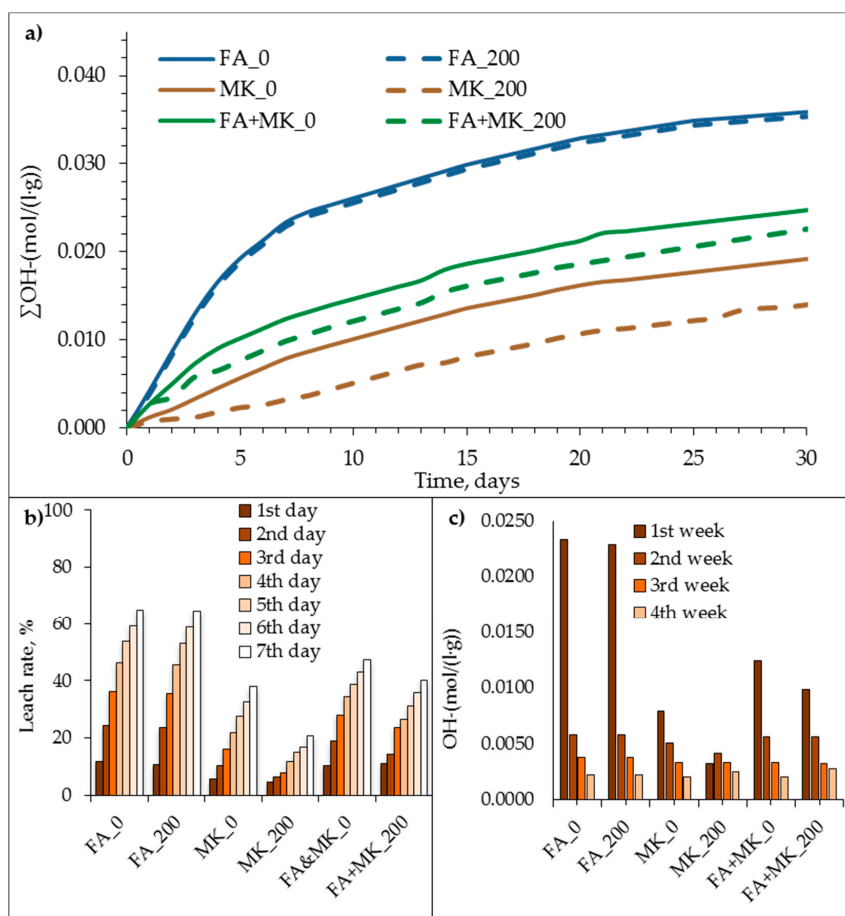


Figure 11. (a) The cumulative leaching rate of OH⁻ ions; (b) OH⁻ ions leached in the first testing week compared to the total leached OH⁻ ions over 35 days; (c) the total amount of OH⁻ per each test week.

The MK + FA_0 and MK + FA_200 showed decrease of total leached amount of OH⁻ ions for 8% — 0.025 (MK + FA_0) — 0.023 (MK + FA_200) mol/(L·g) after 30 days in water media. Heat treatment had no impact on the total amount of OH⁻ ion leached (Figure 11) during the 30 days for samples with FA (FA_0 and FA_200); both of them leached 0.036 mol/(L·g).

The total amount of leached OH⁻ per each test week (Figure 11c) of FA_0 and FA_200 showed that, in the first week, the ion leaching from the structure was more intense. During the first week, 0.023 mol/(L·g) of OH⁻ ions leached from the structure of pAAM with FA (with and without heat treatment). During the second week, only 0.006 mol/(L·g) of OH⁻ ions leached, but during the last week (the fourth week), it was only 0.0022 mol/(L·g). Meanwhile, MK + FA_0 and MK + FA_200 did not show such a sharp reduction in the leached ion amount after the first week compared to pAAM with FA. During the first week, 0.012 mol/(L·g) (MK + FA_0) and 0.010 mol/(L·g) (MK + FA_200) of OH⁻ ions leached from the structure of the pAAM with metakaolin and fly ash mix but during the next three weeks, the leached amount of ions for both types of pAAM was between 0.0020 mol/(L·g) and 0.0056 mol/(L·g). A similar amount of leaching of OH⁻ ions from the structure of MK + FA_0 and MK + FA_200 was detected during the last two weeks of the experiment: Between 0.0020 mol/(L·g) and 0.0033 mol/(L·g).

The pAAM with metakaolin (MK_0 and MK_200) showed relatively similar OH⁻ ion leaching behavior throughout the 30 days of the experiment. However, after the heat treatment, during the first week, ion leaching from the pAAM structure was noticeably less rapid and intensive comparing to pAAM with FA (FA_0 and FA_200). The amount of leached ions from the MK_0 in the first week was 0.0079 mol/(L·g) and it decreased to 0.0032 mol/(L·g) when pAAM was heated at 200 °C before the experiment (MK_200).

The OH⁻ leaching from the pAAM with MK or MK + FA after heat treatment at 200 °C was less intense during the first week; it was smooth and lasted longer, which was the main purpose of the experiment, to prepare this material for testing in water treatment systems. According to Figure 11a,c, the leaching process of samples with MK may have continued after day 30 and it was close to the linear curve.

Since the most intense leaching was detected during the first week of the experiment for pAAM containing FA, the percentage of the leached OH⁻ during the respective time period was calculated (Figure 11b). In the first seven days, samples with fly ash (FA_0) leached up to 65% from the total OH⁻ ion amount leached during the 30-day period, while samples with metakaolin (MK_0) leached only up to 41%; samples with the FA and MK blend (MK + FA_0) leached up to 50% (Figure 11b). As mentioned previously, the heat treatment changed the leaching intensity for the pAAM containing MK. The steadiest OH⁻ leaching was observed in sample MK_200 during the first week (Figure 11b) and during the whole testing period (Figure 11c).

These values are quite similar to the ones of pAAM with red mud and metakaolin presented by Ascensao et al. [47]. Depending on the initial chemical composition, in the first seven days of the experiment, pAAM with red mud and metakaolin presented 0.020–0.055 mol/(L·g) leaching of OH⁻ ions; meanwhile, pAAM with metakaolin and biomass fly ash studied by Novais et al. [5] during the first seven days presented the leaching of OH⁻ ions with a range of 0.005–0.014.

The increased amount of OH⁻ ions leached from the samples with MK or FA and MK blend depended not only on the free alkalis (Na⁺) present in the structure of pAAM but also from the zeolites and N-A-S-H gel that formed during the curing process of the pAAM. Although samples with MK had higher water absorption than samples with FA (which provided better water contact with the pAAM porous surface), they did not have a higher amount of OH⁻ leaching from the structure, resulting from contact with the water (Figure 11).

The total initial OH⁻ ion leaching rate for samples with FA was higher than for samples with MK or MK + FA (Figure 11). However, because the EDX (Figure 8) clearly shows that samples with MK and MK + FA had more sodium in their structure to provide ion exchange, it was concluded that the

samples based on MK can be considered as a material that can ensure high pH in water media for a long period of time.

The leaching results showed that zeolites 4A and analcime could prolong and equate OH^- ion leaching over time; MK_0 and MK + FA_0 showed a more equal leaching rate of OH^- for 30 days. The behavior of the leaching rate of OH^- of FA_0 containing chabazite showed that in the first five days the OH^- leaching was more intense compared with other samples and that leaching intensity reduced significantly after day 5. A meaningful indicator for the description of leaching behavior is the leaching rate of OH^- ions out of the pAAM over a prolonged period of time, but the dynamics of OH^- leaching were not an appropriate indicator in this case.

In addition to the chemical composition, the zeolite formation process can also be controlled by pressure, temperature, the time of the synthesis process, and the pH of the solution (mineralizer amount) [48]. The time, temperature, and pressure in this case were the same for all the samples but the amount of sodium silicate (mineralizer) was different. Raw materials (chemical and mineralogical composition) impacted the type of zeolites formed during the pAAM curing.

It can be argued that heat treatment impacted leaching behavior, mainly depending on the L/S ratio (Table 2) because leaching relied strongly on the chemical composition of pAAM. Higher amounts of the activator used for pAAM production provided a higher number of alkalis that can be leached.

4. Conclusions

The bulk density of the pAAM depended on the aluminum silicate source used. The pAAM made of fly ash had a higher bulk density (up to 750 kg/m^3), while that of pAAM made of metakaolin was lower (up to 490 kg/m^3).

The compressive strength of the pAAM mainly depended on its bulk density and mineralogical composition. Following immersion in water for seven days, it was discovered that there was an increase in the compressive strength of the pAAM and softening of the material did not occur. This provides an advantage in using it in water treatment systems for prolonged periods of time. Zeolites increased the pH-stabilizing capacity of the pAAM to ensure longer and more stable pH adjustments in water media. Therefore, there is scope for further study on these two issues.

The chemical composition of raw materials (aluminum silicate sources), as well as $\text{SiO}_2/\text{Na}_2\text{O}$ and $\text{Al}_2\text{O}_3/\text{Na}_2\text{O}$ ratios, could influence the rate of formation of zeolites in the structure of the pAAM, along with their type, size, and amount.

Heat treatment did not have an impact on the mineralogical composition and structural properties of the pAAM, but it did change the leaching ability of alkalis from the material structure.

The leaching of OH^- ions from the structure of the pAAM could be described by the following properties: The type of aluminum silicate source (FA, MK, or MK + FA); the liquid/solid ratio that directly impacts upon the amount of Na^+ pore solution of the pAAM; and the obtained zeolite type, size, and amount during the alkali-activation process. The pAAM with FA only, due to its mechanical and leaching properties, was not suitable for water treatment systems as a passive pH-controlling system, but potentially could be used as a lightweight, self-supporting construction material.

The pH stabilization in various water systems is important for the efficient operation (chemical and biological treatments). To consider pAAM as acceptable as pH stabilizers for water media, material has to provide stable alkaline water media for a prolonged time period. As the heat treatment of the pAAM containing MK or MK + FA promotes the leaching of OH^- ions for prolonged periods of time, this quality, in combination with a relatively high pH (10.5 after a 30-day leaching test period), makes MK_200 potentially usable in water treatment systems as a passive pH-controlling method, ensuring a pH of 10.6–10.8 for 30 days.

Author Contributions: Conceptualization, L.V. and A.F.-J.; methodology, L.V. and A.F.-J.; investigation, L.V. and A.F.-J.; resources, A.P. and A.F.-J.; writing—original draft preparation, L.V.; writing—review and editing, L.V., D.B., and A.F.-J.; visualization, L.V.; supervision, D.B., A.P., and A.F.-J.; founding acquisition, A.P. and A.F.-J. All authors have read and agreed to the published version of the manuscript.

Funding: This research was supported by Ministry of Economy, Industry and Competitiveness of Spain under the project [BIA2016-76466-R], Riga Technical University (Latvia) Erasmus+ projects [No 2016-1-LV01-KA103-022512 and No 2015-1-LV01-KA103-013255], and Riga Technical University's Doctoral Grant Program.

Conflicts of Interest: The authors declare no conflict of interest.

References

1. Loyd, M.R. Global water security. In *Selected Issues in Water Resources and Management*; Nova Science Publishers: Hauppauge, NY, USA, 2013; pp. 1–30. ISBN 9781629484563.
2. Rugele, K.; Bumanis, G.; Bajare, D.; Lakevics, V.; Rubulis, J. Alkaline Activated Material for pH Control in Biotechnologies. *Key Eng. Mater.* **2014**, *604*, 223–226. [[CrossRef](#)]
3. Bajare, D.; Bumanis, G. Alkali diffusion in porous alkali activated materials. In Proceedings of the NTCC International Conference on Non-Traditional Cement and Concrete, Brno, Czech Republic, 16–19 June 2014; pp. 1–9.
4. Gruskevica, K.; Bumanis, G.; Tihomirova, K.; Bajare, D.; Juhna, T. Alkaline activated material as the adsorbent for uptake of high concentration of Zinc from wastewater. *Key Eng. Mater.* **2016**, *721*, 123–127. [[CrossRef](#)]
5. Novais, R.M.; Buruberri, L.H.; Seabra, M.P.; Bajare, D.; Labrincha, J.A. Novel porous fly ash-containing geopolymers for pH buffering applications. *J. Clean. Prod.* **2016**, *124*, 395–404. [[CrossRef](#)]
6. Novais, R.M.; Seabra, M.P.; Labrincha, J.A. Porous geopolymer spheres as novel pH buffering materials. *J. Clean. Prod.* **2017**, *143*, 1114–1122. [[CrossRef](#)]
7. Provis, J.L. Geopolymers and other alkali activated materials: Why, how, and what? *Mater. Struct.* **2014**, *47*, 11–25. [[CrossRef](#)]
8. Pacheco-Torgal, F.; Castro-Gomes, J.; Jalali, S. Alkali-activated binders: A review Part 1. Historical background, terminology, reaction mechanisms and hydration products. *Constr. Build. Mater.* **2008**, *22*, 1305–1314. [[CrossRef](#)]
9. Lloyd, R.R.; Provis, J.L.; Van Deventer, J.S.J. Pore solution composition and alkali diffusion in inorganic polymer cement. *Cem. Concr. Res.* **2010**, *40*, 1386–1392. [[CrossRef](#)]
10. Komnitsas, K.; Zaharaki, D.; Bartzas, G. Effect of sulphate and nitrate anions on heavy metal immobilisation in ferronickel slag geopolymers. *Appl. Clay Sci.* **2013**. [[CrossRef](#)]
11. Bumanis, G.; Bajare, D. The effect of porous alkali activated material composition on buffer capacity in bioreactors. *Int. J. Chem. Nucl. Metall. Mater. Eng.* **2014**, *8*, 1040–1046.
12. Liu, B.; Huang, T.; Zhang, Z.; Wang, Z.; Zhang, Y.; Li, J. The effect of the alkali additive on the highly active Ru/C catalyst for water gas shift reaction. *Catal. Sci. Technol.* **2014**, *4*, 1286. [[CrossRef](#)]
13. Bumanis, G.; Bajare, D. Porous alkali activated materials with slow alkali release dynamic. *Role of composition. Mater. Constr.* **2018**, *68*. [[CrossRef](#)]
14. Hrachovcova, K.; Tisler, Z.; Svobodová, E.; Safar, J. Modified alkali activated zeolite foams with improved textural and mechanical properties. *Minerals* **2020**, *10*, 483. [[CrossRef](#)]
15. Stoleriu, S.; Vlasceanu, I.N.; Dima, C.; Badanoiu, A.I.; Voicu, G. Alkali activated materials based on glass waste and slag for thermal and acoustic insulation. *Mater. Constr.* **2019**, *69*, 194. [[CrossRef](#)]
16. Vegere, K.; Vitola, L.; Argalis, P.P.; Bajare, D.; Krauklis, A.E. Alkali-activated metakaolin as a zeolite-like binder for the production of adsorbents. *Inorganics* **2019**, *7*, 141. [[CrossRef](#)]
17. Tuff, Z.; Ibrahim, K.M.; Khoury, H.N.; Tuffaha, R. Mo and Ni Removal from drinking water using zeolitic tuff from Jordan. *Minerals* **2016**, *6*, 116. [[CrossRef](#)]
18. Teresa, M.; Deng, S. Ce–Fe-modified zeolite-rich tuff to remove Ba²⁺-like 226Ra²⁺ in presence of As (V) and F[−] from aqueous media as pollutants of drinking water. *J. Hazard. Mater.* **2016**, *302*, 341–350. [[CrossRef](#)]
19. Dessalegne, M.; Diaz, I. Aluminum hydroxide supported on zeolites for fluoride removal from drinking water. *J. Chem. Technol. Biotechnol.* **2016**, *92*, 605–613. [[CrossRef](#)]
20. Minkiewicz, J.; Mozgawa, W.; Kr, M. IR spectroscopy studies of zeolites in geopolymeric materials derived from kaolinite. *J. Mol. Struct.* **2016**, *1126*, 200–206. [[CrossRef](#)]
21. Criado, M.; Fernandez-Jimenez, A.; De La Torre, A.G.; Aranda, M.A.G.; Palomo, A. An XRD study of the effect of the SiO₂/Na₂O ratio on the alkali activation of fly ash. *Cem. Concr. Res.* **2007**, *37*, 671–679. [[CrossRef](#)]
22. Duxson, P.; Fernandez-Jimenez, A.; Provis, J.L.; Lukey, G.C.; Palomo, A.; Van Deventer, J.S.J. Geopolymer technology: The current state of the art. *J. Mater. Sci.* **2007**, *42*, 2917–2933. [[CrossRef](#)]

23. Pablo, J.; Campbell, K.M.; Kane, T.J.; Shoemaker, R.K.; Srubar, W.V. Cement and Concrete Research Mineralization dynamics of metakaolin-based alkali-activated cements. *Cem. Concr. Res.* **2017**, *94*, 1–12. [[CrossRef](#)]
24. Pitcher, S.K.; Slade, R.C.T.; Ward, N.I. Heavy metal removal from motorway stormwater using zeolites. *Sci. Total Environ.* **2004**, *334–335*, 161–166. [[CrossRef](#)] [[PubMed](#)]
25. Zamzow, M.J.; Eichbaum, B.R.; Sandgren, K.R.; Shanks, D.E. Removal of heavy metals and other cations from wastewater using zeolites. *Sep. Sci. Technol.* **1990**, *25*, 1555–1569. [[CrossRef](#)]
26. Bumanis, G.; Novais, R.M.; Carvalheiras, J.; Bajare, D.; Labrincha, J.A. Metals removal from aqueous solutions by tailored porous waste-based granulated alkali-activated materials. *Appl. Clay Sci.* **2019**, *179*, 105147. [[CrossRef](#)]
27. Cooney, E.L.; Booker, N.A. Ammonia removal from wastewaters using natural Australian zeolite. II pilot-scale study using continuous packed column process. *Sep. Sci. Technol.* **1999**, *34*, 2741–2760.
28. Bumanis, G.; Vitola, L.; Fernandez-Jimenez, A.; Palomo, A.; Bajare, D. The Effect of Heat Treatment on Alkali Activated Materials. *Medziagotyra* **2017**, *23*, 266–272. [[CrossRef](#)]
29. Bai, C.; Colombo, P. High-porosity geopolymer membrane supports by peroxide route with the addition of egg white as surfactant. *Ceram. Int.* **2017**, *43*, 2267–2273. [[CrossRef](#)]
30. Bajare, D.; Bumanis, G.; Korjakins, A.; Sele, L. Reuse of non-metallic residues from aluminium recycling industry in production of porous building materials. In *Construction Materials and Structures*; Riga Technical University: Riga, Latvia, 2014; Volume 1, pp. 136–144.
31. Strozi, M.; Colombo, P.; Raymundo, M. Geopolymer foams by gelcasting. *Ceram. Int.* **2014**, *40*, 5723–5730. [[CrossRef](#)]
32. Korat, L.; Ducman, V. The influence of the stabilizing agent SDS on porosity development in alkali-activated fly-ash based foams. *Cem. Concr. Compos.* **2017**, *80*, 168–174. [[CrossRef](#)]
33. Bajare, D.; Vitola, L.; Dembovska, L.; Bumanis, G. Waste stream porous alkali activated materials for high temperature application. *Front. Mater.* **2019**, *6*. [[CrossRef](#)]
34. Horvat, B.; Ducman, V. Potential of green ceramics waste for alkali activated foams. *Materials* **2019**, *12*, 3563. [[CrossRef](#)] [[PubMed](#)]
35. ASTM International. *Standard Specification for Coal Fly Ash and Raw or Calcined Natural Pozzolan for Use in Concrete*; ASTM International: West Conshohocken, PA, USA, 2012.
36. Ruiz-Santaquiteria, C.; Fernández-Jimenez, A.; Skibsted, J.; Palomo, A. Clay reactivity: Production of alkali activated cements. *Appl. Clay Sci.* **2013**, *73*, 11–16. [[CrossRef](#)]
37. Bumanis, G.; Vitola, L.; Bajare, D.; Dembovska, L.; Pundiene, I. Impact of reactive SiO₂/Al₂O₃ ratio in precursor on durability of porous alkali activated materials. *Ceram. Int.* **2017**, *43*, 5471–5477. [[CrossRef](#)]
38. American Society for Testing and Materials International ASTM (2009). Standard Test Method for Density of Hydraulic Cement. *Annu. B. ASTM Stand.* **2017**. [[CrossRef](#)]
39. Pacheco-Torgal, F.; Labrincha, J.A.; Leonelli, C.; Palomo, A.; Chindaprasirt, P. *Handbook of Alkali-Activated Cements, Mortars and Concretes*; Elsevier: Amsterdam, The Netherlands, 2014; ISBN 9781782422884.
40. Zhang, Z.; Wang, H.; Provis, J.L.; Bullen, F.; Reid, A.; Zhu, Y. Quantitative kinetic and structural analysis of geopolymers. Part 1. The activation of metakaolin with sodium hydroxide. *Thermochim. Acta* **2012**, *539*, 23–33. [[CrossRef](#)]
41. Garcia-Lodeiro, I.; Fernandez-Jimenez, A.; Blanco, M.T.; Palomo, A. FTIR study of the sol-gel synthesis of cementitious gels: C-S-H and N-A-S-H. *J. Sol. Gel. Sci. Technol.* **2008**, *45*, 63–72. [[CrossRef](#)]
42. Criado, M.; Palomo, A.; Fernandez-Jimenez, A. Alkali activation of fly ashes. Part 1: Effect of curing conditions on the carbonation of the reaction products. *Fuel* **2005**, *84*, 2048–2054. [[CrossRef](#)]
43. Lee, W.K.W.; van Deventer, J.S.J. Use of infrared spectroscopy to study geopolymerization of heterogeneous amorphous aluminosilicates. *Langmuir* **2003**, *19*, 8726–8734. [[CrossRef](#)]
44. Fernandez-Jimenez, A.; Palomo, A. Mid-infrared spectroscopic studies of alkali-activated fly ash structure. *Microporous Mesoporous Mater.* **2005**, *86*, 207–214. [[CrossRef](#)]
45. Fernandez-Jimenez, A.; Garcia-Lodeiro, I.; Palomo, A. Durability of alkali-activated fly ash cementitious materials. *J. Mater. Sci.* **2007**, *42*, 3055–3065. [[CrossRef](#)]
46. Hong, S.Y.; Glasser, F.P. Alkali sorption by C-S-H and C-A-S-H gels: Part II. Role of alumina. *Cem. Concr. Res.* **2002**, *32*, 1101–1111. [[CrossRef](#)]

47. Ascensano, G.; Seabra, M.P.; Aguiar, J.B.; Labrincha, J.A. Red mud-based geopolymers with tailored alkali diffusion properties and pH buffering ability. *J. Clean. Prod. J.* **2017**, *148*, 23–30. [[CrossRef](#)]
48. Querol, X.; Moreno, N.; Umaña, J.T.; Alastuey, A.; Hernández, E.; Lopez-Soler, A.; Plana, F. Synthesis of zeolites from coal fly ash: An overview. *Int. J. Coal Geol.* **2002**, *50*, 413–423. [[CrossRef](#)]

Publisher’s Note: MDPI stays neutral with regard to jurisdictional claims in published maps and institutional affiliations.



© 2020 by the authors. Licensee MDPI, Basel, Switzerland. This article is an open access article distributed under the terms and conditions of the Creative Commons Attribution (CC BY) license (<http://creativecommons.org/licenses/by/4.0/>).